Evaluating Void Fraction Models for Two-Phase Flow in Microchannels

Jackson Sammartino ©2024

Abstract

The accurate prediction of two-phase flow properties, including void fraction α, is critical for optimizing the design and functionality of two-phase flow systems, particularly in microchannel applications where phase-change heat transfer can be leveraged for ideal thermal management. This study evaluated various types of void fraction models, including the homogeneous flow model, slip ratio correlations (Chisholm correlation), drift flux models (Chen, Twu, and Pan correlation), and the Armand empirical correlation, to identify the best predictive model for adiabatic two-phase flow in a 300 μm circular microchannel. Experimental data for air (0.08-1.5 m/s) and deionized water (0.08-1.5 m/s) were collected at homogeneous void fractions β varying from 0.05 to 0.95 and slip ratios S varying from 0.053-19. The results, mainly in the intermittent/slug flow regime, showed significant differences in model performance. The Armand correlation, $\alpha = 0.833\beta$, had the lowest root-mean-square error of 0.07154 and the strongest linear correlation with experimental data (R^2 value of 0.984), outperforming the other models across the full range of test conditions. The homogeneous flow model mostly overpredicted α in the separated flow regimes, while the slip ratio and drift flux models demonstrated limited versatility across ranges of β and S. Furthermore, the study identified no significant impact of axial location on void fraction within the tested channel size and flow conditions, though this effect may become relevant in channels smaller than ~275 μm. These findings emphasized the versatility of the Armand correlation, and that the influence of specific flow mechanisms like velocity slip, velocity drift, buoyancy, etc. under the tested conditions were not strong enough to warrant use of a specialized void fraction model. Future research should extend this evaluation to additional channel geometries, smaller channels, and all flow regimes to establish definitive applicability limits for each model.

Key Words: adiabatic two-phase flow, flow regimes, microchannels, void fraction

Table of Contents

Nomenclature

A	Area, m^2
C	Experimental constant: $\dot{m}_{air}R_{air}T$
D	Channel diameter, m or μm
f	Darcy friction factor
k	Experimental constant: $128\mu Q_l^2/\pi D^4 C$
L	Channel length, m or cm
$\dot{m}$	Mass flow rate, kg/s
n	Number of experimental data points
P	Pressure, Pa
Q	Volumetric flow rate, m^3/s
R	Gas constant, J/kg/K
r	Correlation coefficient
r^2	Coefficient of determination
Re	Reynolds number: $\rho UD/\mu$
$RMSE$	Root-mean-square error
S	Gas-liquid velocity slip ratio: U_g/U_l
t	Time, s
T	Temperature, K
U	Superficial velocity, m/s
$\overline{U}$	Average U, m/s
x	Axial position, m
X	Flow quality: $\dot{m}_g/\dot{m}_{total}$

Greek Symbols

α	Void fraction
β	Homogeneous α: Q_g/Q_{total}
δ	Thin liquid film thickness, m
Δ	Length of time window, s
ρ	Fluid density, kg/m^3
μ	Fluid viscosity, Pa×s
μ_i	Uncertainty value

Subscripts

total	Total of both phases
g	Gas
air	Air
l	Liquid
2phase	Two-phase property
bubble	Bubble property
i	Index
top	Film on top of channel
bottom	Film on bottom of channel
atm	Atmospheric conditions
measured	Measured value in experiment
predicted	Predicted value by model

1. Introduction

1.1 Overview of Applications

With the rapidly increasing capabilities of computational technology- for instance, integrated circuits, computer chips, and artificial intelligence- comes a high demand for and consumption of power. The most significant limiting factor in the way of the advancement of these technologies is thermal management- specifically, removal of waste heat generated during operation [1]. An effective, but still developing, method for cooling these devices is phase-change heat sinks, which employ two-phase flow of a gas and liquid phase to absorb far more heat than air-fan or liquid cooling systems. As shown in Figure 1 below, two-phase flow allows electronics to remain at lower temperature levels than with traditional single-phase cooling methods [2]. Heat transfer coefficients on the order of 1 MW/m^2/K have been achieved in such systems [3]. These results are especially promising in data centers, which are quickly increasing in size and density to meet worldwide demands [1].

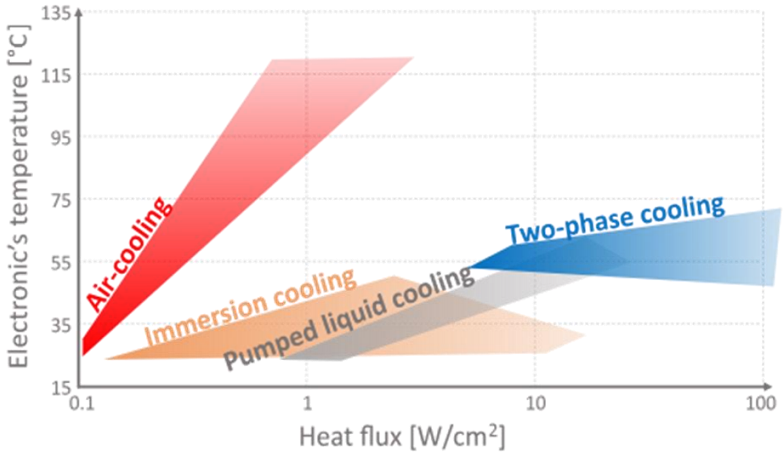

Fig. 1: Effectiveness of different types of cooling methods, *JJ Cooling Solutions*, 2024 [2].

The potential of two-phase flow for enabling further evolution of electronic devices cannot be understated; thus, it is equally important to invest in research that establishes a wide and reliable understanding of the underlying microscale science. Accurate models are needed for optimal design of microscale two-phase systems, which will help in overcoming the barrier of thermal management and permit further technological advancement.

1.2 Flow Regimes

Two essential characteristics of any two-phase flow system are the flow regime and the void fraction, α. The flow regime determines the behavior of the flow, including heat transfer capability. Flow regimes have been quite thoroughly studied, and although there is not absolute consensus in the literature, there are at least four majorly agreed-upon regimes. Slug flow is characterized by intermittent movement of elongated bubbles separated by intermittent liquid slugs, and occurs at low gas and low liquid velocities (U_{gas} and U_{liquid}, respectively). As the velocity of the gas phase increases, the two phases become more mixed, resulting in bubbly flow. Similarly, churn flow occurs at high gas and high liquid velocities, with regions of highly mixed phases and long bubbles. Annular flow, which occurs at low gas and high liquid velocities, consists of a gas core surrounded by a thin, ring-like liquid film. Numerous flow regime maps have been created with good reliability, as abbreviated in Figure 2 below [4]. It is essential to consider the influence of flow regimes on the void fraction α.

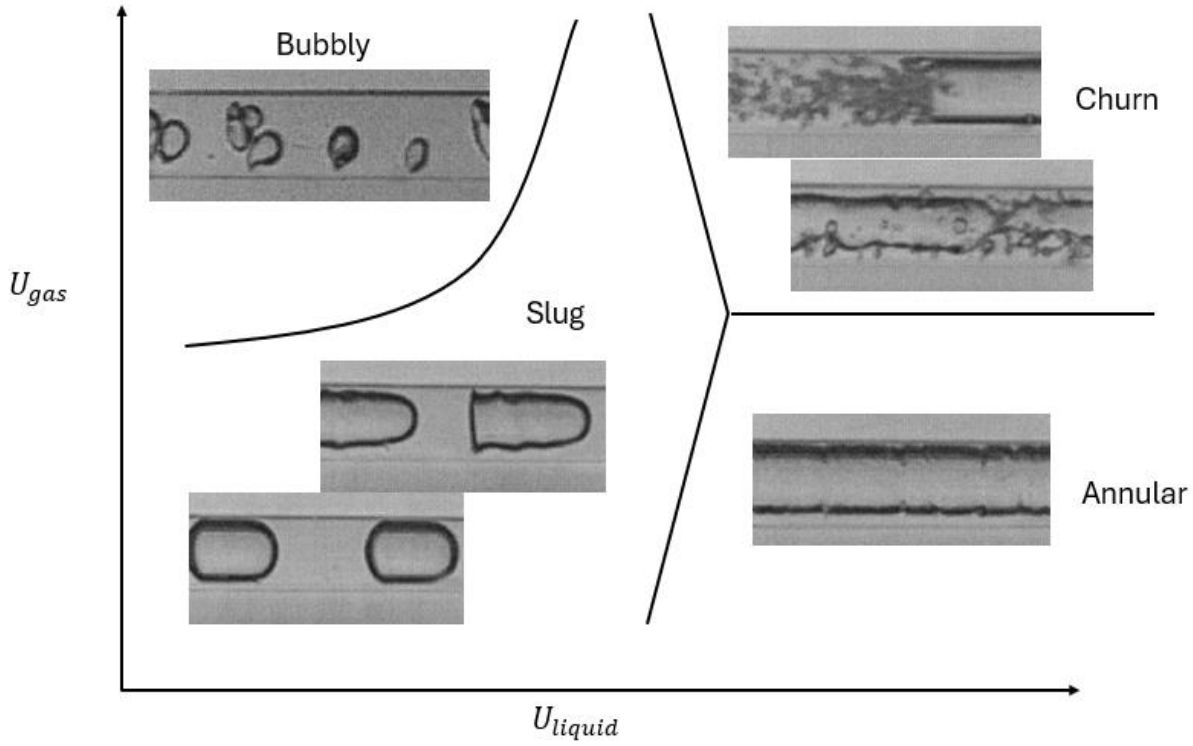

Fig. 2: Example flow regime map, *adapted from Triplett et al.* [4].

1.3 Void Fraction

Void fraction α, defined as the time-averaged proportion of a channel occupied by the gas phase and illustrated in Figure 3 below, is the primary focus of this work. Void fraction is a more difficult property to predict due to the balance of forces, flow regimes, and two-phase properties in a microchannel; it can be used to estimate the average liquid film thickness in two-phase flow, as well as the pressure drop in two-phase systems [4], [5]. Several different categories of void fraction models, each with varying assumptions and numerous empirical correlations, have been developed to predict void fraction in two-phase flow.

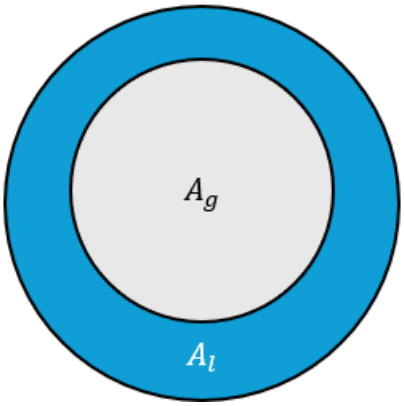

Fig. 3: Axial view of two-phase flow showing void fraction. It is important to note that the gas core is almost almost always assumed axisymmetric in microchannels, while the outer liquid ring need not be.

$$\alpha = \frac{A_g}{A_{total}} = \frac{A_g}{A_g + A_l}$$

Other parameters relevant to void fraction are the homogeneous void fraction β (the volumetric proportion of gas flow), and slip ratio S (the ratio of superficial gas velocity to superficial liquid velocity), both defined below. The predicted or actual void fraction α is often correlated to one or both of these values, in addition to other flow mechanisms.

$$\beta = \frac{Q_g}{Q_{total}} = \frac{Q_g}{Q_g + Q_l}$$

$$S = \frac{U_g}{U_l}$$

1.4 Homogeneous Flow Model

The simplest method of void fraction calculation is via the homogeneous flow model. Under this model, the two phases are assumed to be continuous and perfectly mixed such that they behave as one phase. Thus, they move at the same velocity U with no velocity slip between phases ($S = 1$). Given these assumptions, the following formulation results.

$$\beta = \frac{Q_g}{Q_g + Q_l} = \frac{UA_g}{UA_g + UA_l} = \frac{A_g}{A_g + A_l} = \alpha$$

Thus, this models predicts that the actual void fraction α is equal to the homogeneous void fraction β, hence the name. Using air at velocities of 0.02-80 m/s and water at velocities 0.02-8 m/s, Triplett et al. found that this model performed the best in channels of diameters 1.1 mm and 1.45 mm [5]. They found the homogeneous flow model to be especially accurate for bubbly and slug flow, while overpredicting α for other flow regimes (churn) [5]. Chen, Twu, and Pan, however, performed tests on a similar scale with nitrogen and water, finding the homogeneous flow model ineffective compared to their developed drift-flux model [6]. Under similar flow conditions, but in much smaller channels of diameter ~100 μm, Kawahara, Chung, and Kawaji observed significant overpredictions for intermittent slug flow due to large slip ratios between phases [7], [8]. The homogeneous flow model's reliability is certainly in question, especially with regards to how well it can predict α in highly separated flow regimes with high slip ratios, and in microchannels under 1 mm in diameter.

1.5 Slip Ratio Models

In contrast to the homogeneous flow model, slip ratio models account for the influence of S on α in microchannels. A prominent slip ratio correlation was developed by Chisholm and Rooney, which factors in flow quality X (the mass proportion of gas flow) and fluid densities ρ, as defined below [9].

$$X = \frac{\dot{m}_g}{\dot{m}_{total}} = \frac{\dot{m}_g}{\dot{m}_g + \dot{m}_l}$$

$$\alpha = \left[1 + \left(\frac{1 - X}{X}\right)\left(\frac{\rho_g}{\rho_l}\right)\sqrt{1 - X\left(1 - \frac{\rho_l}{\rho_g}\right)}\right]^{-1}$$

Although this model introduces more complexity than the homogeneous flow model, it offers predictive value when the velocities of the two phases differ significantly. However, this seems to come at the cost of versatility. He et al. found that, although the Chisholm correlation was the best overall model for a microchannel, it was highly inconsistent across different ranges of β, being most accurate for $0.7 < \beta < 1$ [10]. Woldesemayat and Ghajar's vast survey of data from the literature corroborated this finding, concluding that linear-type models gave more accurate predictions across all microchannels and flow conditions [11]. Thus, the versatility of slip ratio models across β at varying S is uncertain.

1.6 Drift Flux Models

Another factor neglected by other models, but considered important in some cases, is buoyancy. Drift flux models, most notably developed by Chen, Twu, and Pan, assume a constant drift velocity between the gas phase U_g and the overall two-phase velocity U_{2phase} due to buoyant forces: their formulation and resulting correlation are shown below [6].

$$U_{2phase} = \frac{Q_{total}}{A_{total}} \rightarrow U_{bubble} = 0.932\left(U_{2phase}\right)^{1.1} \rightarrow \alpha = \frac{U_g}{U_{bubble}}$$

$$for\ 0.5 \leq U_{2phase} \leq 8\ m/s$$

Studies indicate that this type of model may be favorable in annular flow regimes in larger channels (> 1 mm); however, in the majority of microscale internal flow, the force of buoyancy is negligible relative to surface tension and viscosity [12], [13]. This model's validity in microchannels is to be determined, specifically the lower channel size limit.

1.7 Other Empirical Correlations

Following no particular assumptions, there are innumerable empirical void fraction equations in the literature, most of which predict α based on β. The most prominent is that of Armand and Treschev: a simple linear relationship shown below [14].

$$\alpha = 0.833\beta$$

While there are variations of this equation that use slightly different values for the β coefficient and intercept, the original Armand correlation has shown high predictive capabilities in microchannels. Serizawa, Feng, and Kawara tested air and water velocities up to 295 and 17.5

m/s, respectively, and found that the Armand correlation performed well across all flow regimes in channels as small as 25 μm [15]. Chung and Kawaji also found good agreement, but only down to a 250 μm channel [16]. Chung et al. determined that void fraction behavior in a 96 μm square microchannel was highly non-linear, favoring a slip ratio model instead [17]. The Armand correlation could be a versatile predictor above 250 μm, but the limit of its accuracy in smaller microchannels is not clear.

1.8 Summary of Study

Uncertainty remains as to which void fraction model is best suited for a given microchannel and set of flow conditions. In this study, an experiment is designed to test each model at a wide range of β and S. The accuracy of the homogeneous flow model is tested for separated flows with high velocity slip, in channels < 1 mm. The consistency of slip ratio models, specifically the Chisholm correlation, are tested across the full range of β [9]. A (lower) channel size limit for the influence of buoyancy and the accuracy of the Chen et al. drift flux model is sought [6]. The versatility of the Armand correlation is to be determined over a range of flow conditions, and a (lower) channel size limit for its accuracy is sought [14]. The complex influences of flow conditions- fluid properties, flow rates and regimes, and channel diameter- as well as flow mechanisms, like buoyancy and velocity slip, on void fraction are investigated, and the most suitable model determined. Evaluative methods used to answer this inquiry were: generation of correlations for raw data, graphical comparison of raw data to models, and root-mean-square error calculation for each model. A preferrable model is selected and future studies are suggested to address limitations of this study for gaining more certainty of the conclusions.

2. Methodology

2.1 Equipment and Setup

Figure 4 depicts the setup used for this experiment. Air and deionized water, both thermally equilibrated with the ambient room (STP) to ensure adiabatic conditions, were separately supplied by Fisher Scientific syringe pumps (Fig. 5). Each pump was calibrated to the diameter of its syringe, with the ability to provide a maximum flow rate of 417.6 mL/hr. The two phases joined in plastic tubing and flowed through a 300 μm diameter glass channel of length 10 cm (Fig. 6), subsequently discharging at atmospheric pressure P_{atm}. The channel was mounted to

a 3-stage adjuster to easily focus the camera (Photron SA4 FASTCAM), which recorded video of the midpoint of the channel at 10,000 frames per second. A chip-on-board light fixture (Fig. 7) connected to a power source supplied light to the camera.

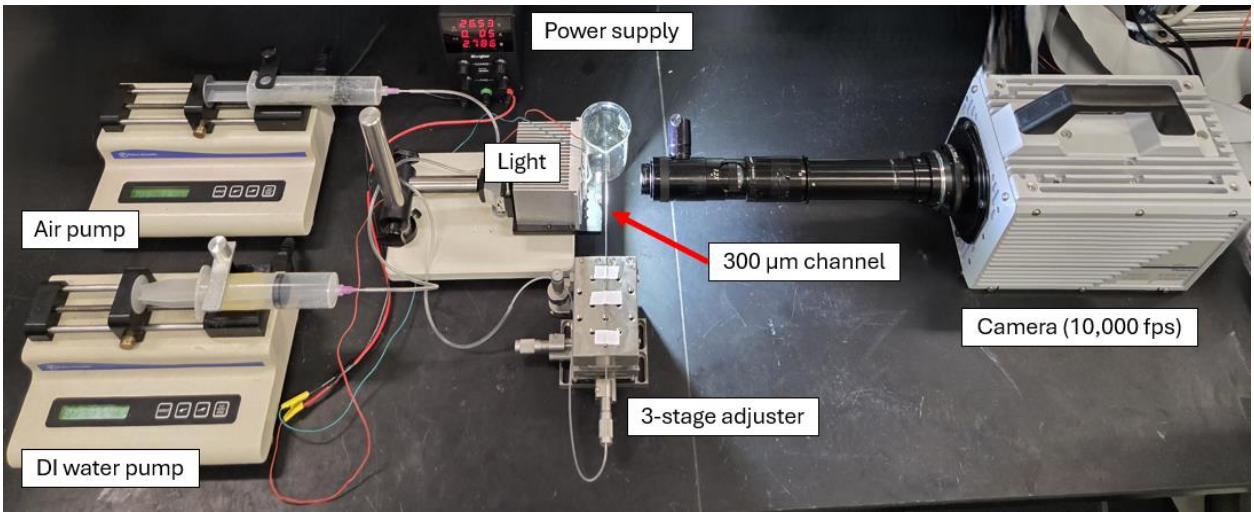

Fig. 4: Experimental setup used for adiabatic two-phase flow.

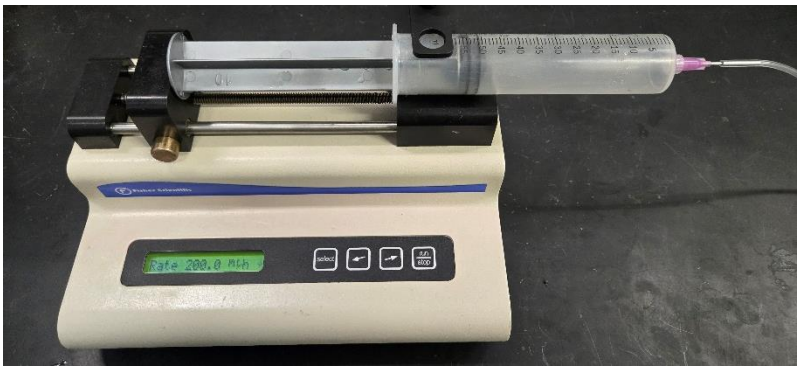

Fig. 5: Fisher Scientific syringe pump.

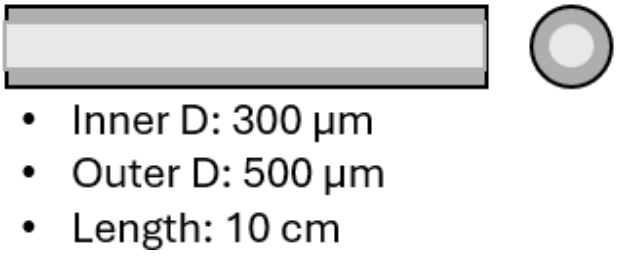

Fig. 6: 300 µm circular channel geometry (not to scale).

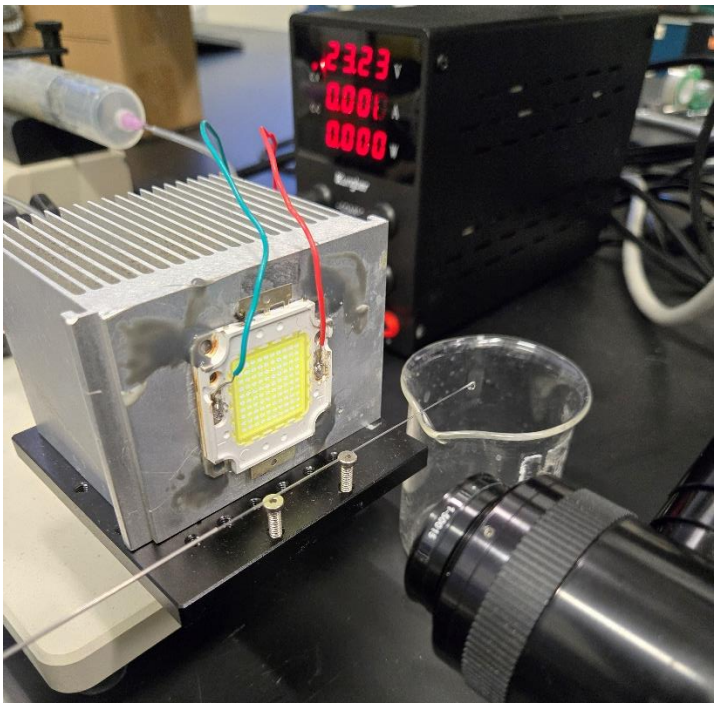

Fig. 7: Chip-on-board light fixture illuminating the channel.

2.2 Procedure

After the fluids were thermally equilibrated, Q_g was set to 380 mL/hr while Q_l was set to 20 mL/hr, for a β of 0.95. The two volumetric flow rates were then altered such that β was lowered to 0.05 in increments of 0.05, while maintaining the sum of Q_g and Q_l at a constant 400 mL/hr. The following ranges of flow conditions were achieved.

$$0.05 \leq \beta \leq 0.95$$

$$0.08 \leq U_g, U_l \leq 1.5\ m/s$$

$$0.053 \leq S \leq 19$$

The system was given time (~3 minutes) to reach a steady flow and consistent flow regime, at which point video was recorded to a computer. It is important to note that for high relative values of Q_l (~above 300 mL/hr), an issue of backflow was observed due to pressure differences. Upon start-up of the syringe pumps, some amount of water flowed backwards into the air syringe, instead of through the channel (Fig. 8). This would certainly confound results; thus, no data was taken until this backflow had completely stopped.

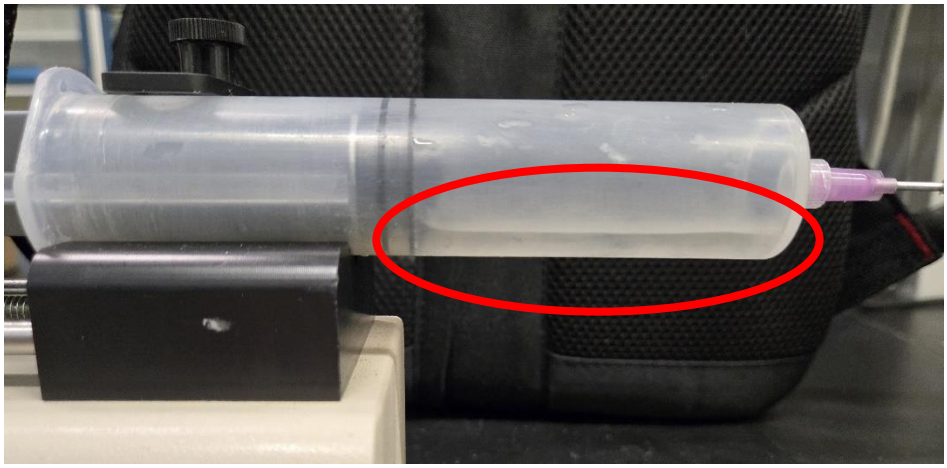

Fig. 8: Backflow in air syringe at high relative liquid flow rates.

2.3 Data Analysis

Spatial measurements were performed in the Photron FASTCAM Viewer 4 software (PFV4). Firstly, a calibration measurement was made, based on an assumed channel diameter of 300 μm. Then, distinct void fractions were measured and calculated across discrete time intervals Δt_i, falling into one of three categories: liquid-only ($\alpha = 0$), gas-only ($\alpha = 1$), or annular/slug bubbles (formula shown below) [7]. Note that although the cross-section of the gas core was assumed to be axisymmetric, the liquid perimeter was not. Figure 9 depicts these measurements visually in the PFV4 software.

$$\alpha = \frac{\left(D - \delta_{top} - \delta_{bottom}\right)^2}{D^2}$$

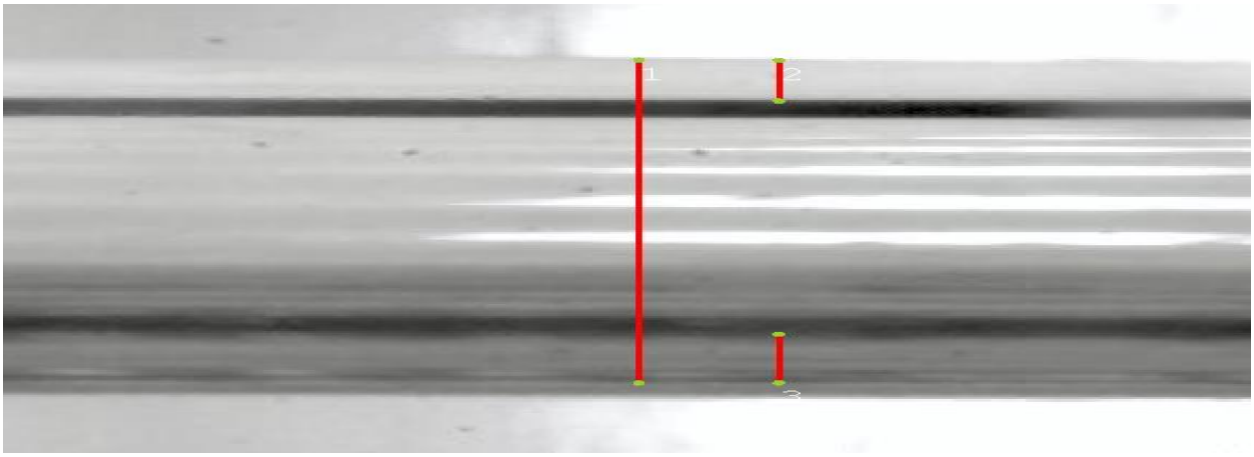

Fig. 9: Side view of measurements being made in PFV4 software (1. calibration, 2. δ_{top}, 3. δ_{bottom}).

Once distinct void fractions had been calculated over discrete time intervals, the following time-averaged formula was applied over the entire length of video [7].

$$\alpha = \frac{\sum \Delta t_i \alpha_i}{\sum \Delta t_i}$$

To ensure the length of video used provided a reasonable average, a halving process was conducted: the first half of the data was isolated and the time-averaged void fraction formula was applied again. These new averages were compared to the initial averages, resulting in marginal differences not exceeding 10%. Thus, the length of video was deemed acceptable for calculating a time-averaged void fraction.

2.4 Uncertainty Analysis

Uncertainty was present in the calibration/resolution of the PFV4 software, the diameter of the channels, and the flow rates of the syringe pumps [18]. The following Table I summarizes these individual uncertainty values, which were propagated to the void fraction formula using the root-sum-square method. The symbolic formulation is shown below, along with the final void fraction uncertainty of 0.0321. This value was sufficiently low and did not interfere with data analysis or make conclusions uncertain.

Table I: Individual Uncertainty Values

Source	**Variables**	**Value**	**Justification**
PFV4 software	δ_{top}, δ_{bottom}	±1 pixel = ±3.41 μm	Calibration [18]
Channel diameter	D	±1.33 μm	Manufacturer [18]
Flow rates	Q_g, Q_l	<1% (neglected)	Manufacturer, self [18]

$$\alpha = \frac{\left(D - \delta_{top} - \delta_{bottom}\right)^2}{D^2}$$

$$\mu_\alpha = \sqrt{\left(\mu_D \frac{\partial \alpha}{\partial D}\right)^2 + \left(\mu_{\delta_{top}} \frac{\partial \alpha}{\partial \delta_{top}}\right)^2 + \left(\mu_{\delta_{bottom}} \frac{\partial \alpha}{\partial \delta_{bottom}}\right)^2} = 0.0321$$

3. Results and Discussion

3.1 Raw Data and Correlations

The resulting videos captured slug and intermittent flow regimes, with occasional bubbly flow (Fig. 2). Figures 10 and 11 depict the raw void fraction data for this experiment with uncertainty bars of 0.0321 in either direction, and a linear correlation. The x-axis is the homogeneous void fraction β and the y-axis is the measured void fraction α. From an initial review, the data appear linear; however, some noteworthy observations arose. The data seem to exhibit hysteresis- a phenomenon in fluid mechanics where the behavior of a system depends on its history. In this case, the history of the system was the order in which the flow rates were altered. The procedure for this study varied the flow rates by decreasing Q_g and increasing Q_l, but executing this process in reverse may lead to different results. This manifested in the data alternating above and below the trendline in a zigzag manner. Still, the linear correlation was very strong, with an R^2 value of 0.984 (R value of 0.992). The α-intercept of the trendline was set to zero in agreement with correlations in the literature, resulting in the trendline $\alpha = 0.8872\beta$.

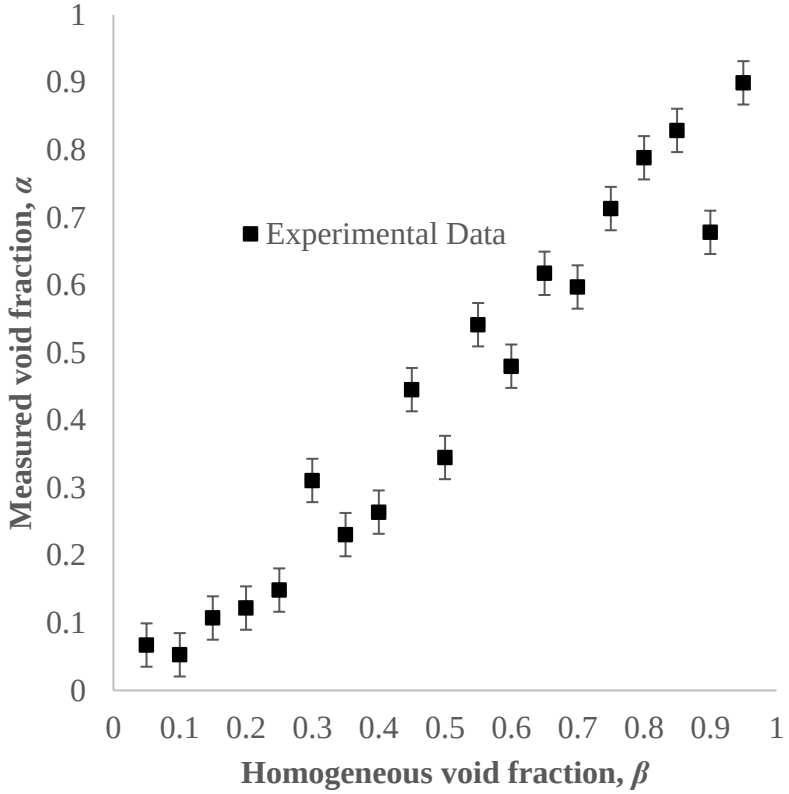

Fig. 10: Raw data with uncertainty bars.

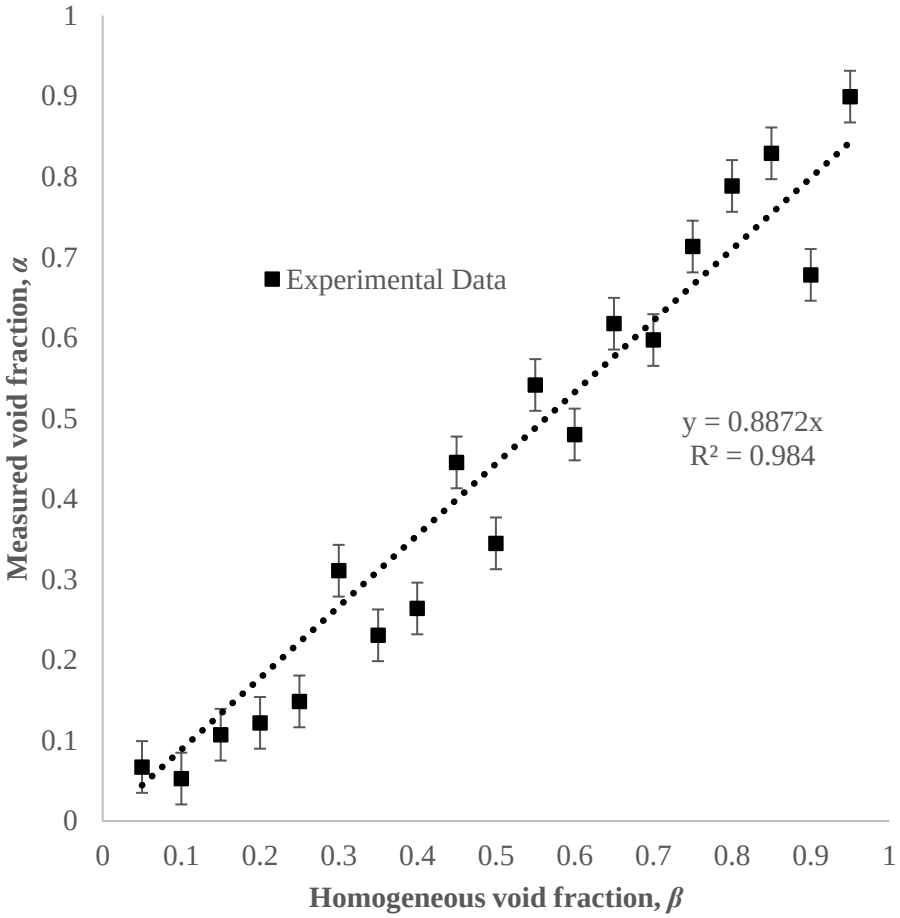

Fig. 11: Raw data with uncertainty bars and linear correlation.

Despite the data appearing highly linear, the behavior near the lower and upper limits of β appeared to deviate slightly. In fact, there appeared to be an *S*-shaped or cubic function that could be used to correlate the data. This behavior would indicate a slip ratio model as a better fit to the data than a linear model; however, the resulting correlation shown in Figure 12 below indicated a slightly weaker correlation (R^2 value of 0.953 and R value of 0.976). Still, more evaluation measures were needed to clarify the best model.

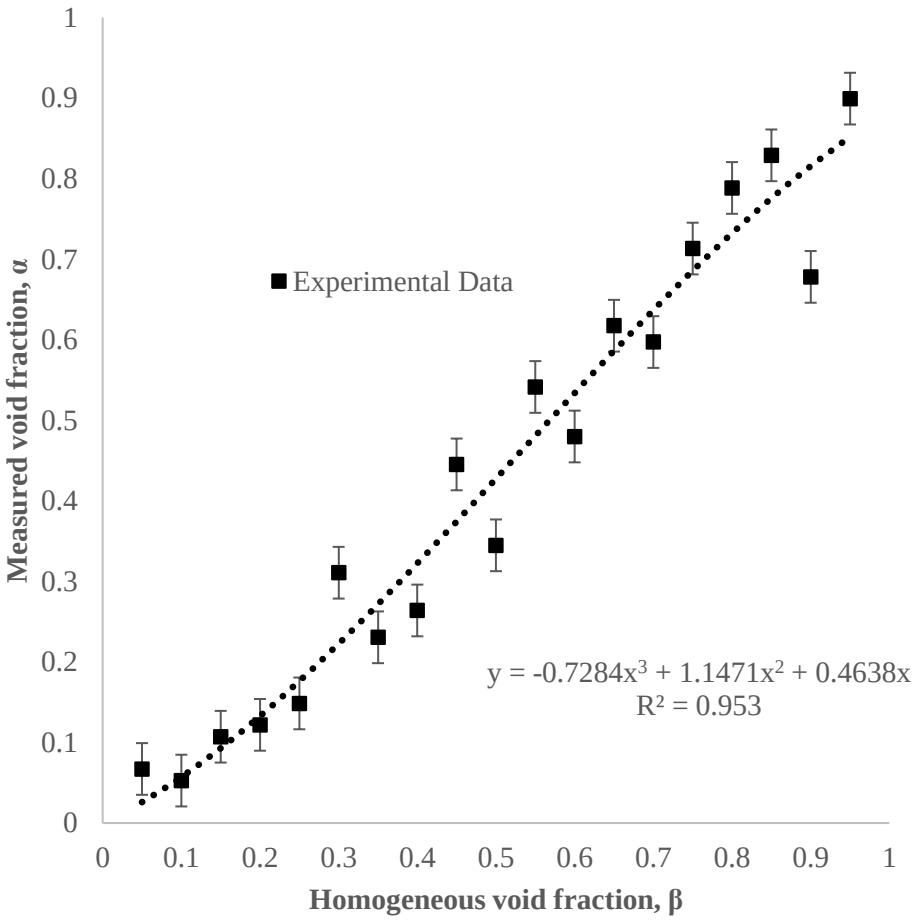

Fig. 12: Raw data with uncertainty bars and cubic correlation.

3.2 Graphical Evaluation of Models

The experimental data were plotted against the different tested void fraction models to gain another evaluative metric for the best model (Fig. 13 below). The Chen et al. drift flux model most overpredicted the experimental data, as did the homogeneous flow model [6]. However, both were more accurate at high values of β, where the phases were more mixed and approaching the bubbly flow regime from the slug flow regime (Fig. 2). The Chisholm slip ratio correlation was quite inconsistent, mostly overpredicting α at lower β with slightly more accuracy, and underpredicting α at higher β [9]. The Armand correlation was fairly accurate across all experimental conditions. Still, it generally overpredicted α at lower β and underpredicted α at higher β. From the graphical analysis, the Armand correlation appeared most favorable.

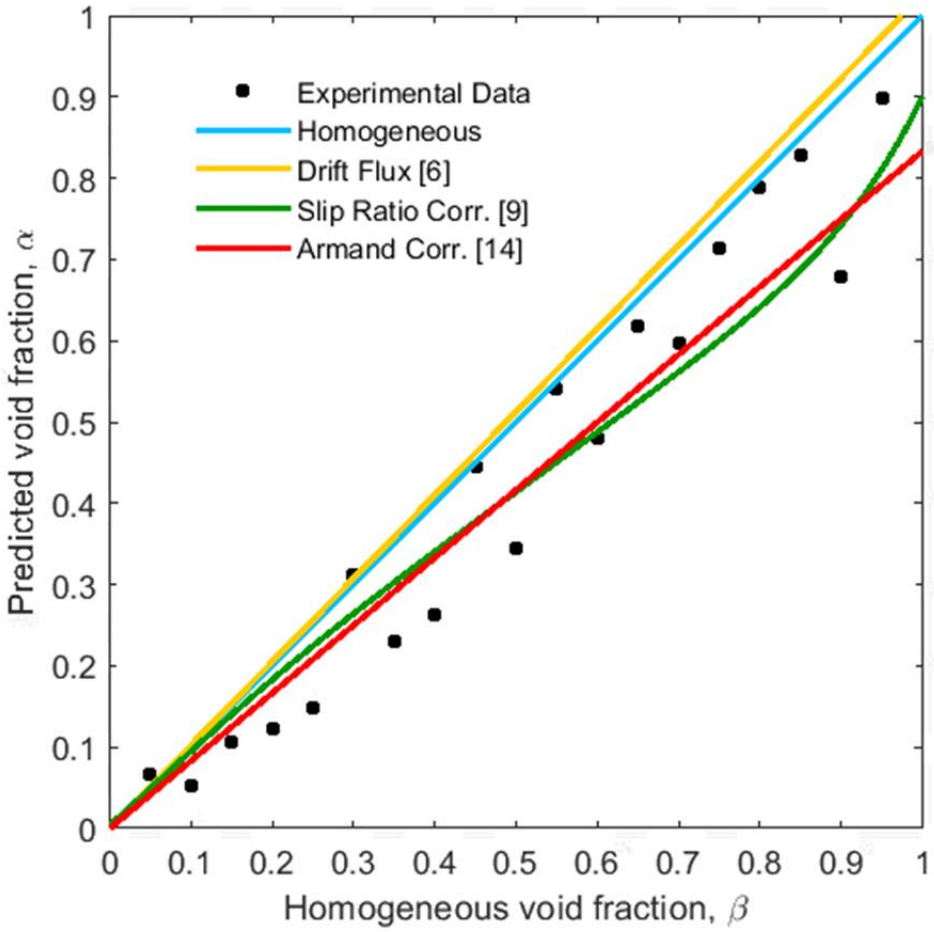

Fig. 13: Raw data plotted against void fraction models.

3.3 RMSE Evaluation of Models

Another metric used to confirm the best void fraction model was root-mean-square error (RMSE), defined below. Table II shows the resulting RMSE for each model ranked from lowest to highest for n = 19 trials. The Armand correlation had the lowest RMSE.

$$RMSE = \sqrt{\frac{\sum\left(\alpha_{measured} - \alpha_{predicted}\right)^2}{n}}$$

Table II: RSME for Each Model

Model	**RMSE**
Armand correlation [14]	0.07154
Chisholm slip ratio correlation [9]	0.07932
Homogeneous flow model	0.09109
Chen et al. drift flux model [6]	0.1019

3.4 Predictive Capabilities of Models

Taking into account the evaluative metrics used in this study- correlations, graphical comparison, and RMSE- each model performed differently. The homogeneous flow model was somewhat inaccurate with an RMSE of 0.9019. It mostly overpredicted void fraction, likely due to the separated phases and intermittent/slug flow regimes observed in this study (Fig. 2). It was more accurate at higher values of β since the phases were slightly more mixed at these conditions [5], [6]. This was an interesting finding because slip ratios corresponding to these conditions were much greater than one (the model assumes $S = 1$). It could be a useful estimator of void fraction at highly mixed bubbly flow regimes, but the extent of this usefulness was not determined. The (lower) channel size limit of its accuracy was not determined, but it could reasonably be stated that a 300 μm circular microchannel was too small for this model.

The Chisholm slip ratio correlation was somewhat inaccurate and inconsistent, with an RMSE of 0.7932 [9]. As reported in the literature, it performed quite differently across β, overpredicting at low values and underpredicting at high values [10]. It was not effective over the full range of β and S tested in a 300 μm channel. It is believed that the effects of slip may be more prominent in smaller channels (~100 μm and smaller) as suggest by some [7], [8], [10]. Despite the data being fairly well-correlated by a cubic (slip ratio) function, the linear correlation was stronger and more versatile across all tested flow conditions [11].

The Chen et al. drift flux model was the worst-performing model, with an RMSE of 0.1019: an order of magnitude greater than the others [6]. Despite the experimental conditions being within the model's limits on two-phase flow velocities, this was a foreseeable result considering the negligible influence of gravity/buoyancy in microchannels [12], [13]. The

(lower) channel size limit for the usefulness of this model was not determined; however, it may be accurate in mini/midi-channels around 1 mm in diameter [13]. It can reasonably be stated that a 300 μm circular microchannel was too small for this model. Generally, it should be not be used for two-phase flow in microchannels less than 1 mm in diameter.

This study revealed the most support for Armand correlation, with the lowest RMSE of 0.07154 and extremely high R^2 value of 0.984. The raw data trendline slope of 0.8872 was within 7% of the Armand coefficient of 0.833 [14]. Just as importantly, the Armand correlation was effective over the full range of β and varying slip ratios. It seemed to accurately capture the combined influence of various flow conditions on void fraction, without requiring any specific mechanisms (slip, buoyancy, flow regime, etc.) to be accounted for. Still, it exhibited some weaknesses by overpredicting at low β and underpredicting at high β. The (lower) channel size limit for its effectiveness was not determined, but it can reasonably be stated that a 300 μm circular microchannel was within the range of this model's accuracy.

3.5 Influence of Axial Location on β

Shown completely in the Appendix, an analytical analysis of void fraction using traditional fluid mechanics equations revealed that the axial location along the microchannel's length may affect the value of β, and thus the value of α. Because the microchannel was free to discharge to P_{atm}, there was significant pressure drop along the channel, which decompressed and therefore expanded the air phase. Using the Darcy-Weisbach pressure loss equation and the ideal gas law applied to the air phase, an axial location term $k(L-x)$ emerged in the equation for β. Thus, β is a function of x, i.e. the axial position. The video data collected for this study was taken at the channel midpoint, so it was important to determine if this variable affected the results. In short, for the flow conditions tested, the influence of this axial location term was calculated to be negligibly small in channels down to ~275 μm in diameter. Thus, it was deemed insignificant for this study. However, it would be relevant in studies of microchannels smaller than this limit; thus, the axial position of the camera should be varied along the length of the channel to accurately account for the compressibility of the air phase.

3.6 Implications

The importance of these findings for slugs/bubbles in a 300 μm microchannel are as follows: there was a strong linear relationship between homogeneous void fraction β and actual void fraction α [11]. This relationship accurately captured the combined effects of fluid properties, flow conditions, and velocity slip on void fraction across the entire range of β and a wide range of slip ratios- better so than the models developed for each of these factors individually [6], [9]. This was an interesting finding that shows the isolated influences of slip, buoyancy, etc. were not strong enough in this regime to warrant the use of a specialized void fraction model- a simple linear correlation was sufficient. Additionally, the effect of axial location on void fraction should be considered in channels smaller than ~275 μm.

3.7 Limitations

Several important limitations to this study are as follows: evidence in support of the Armand correlation does not necessarily prove it. A more broad range of flow regimes, fluids with varying surface tension and viscosity, and especially channel diameters should be tested to gather conclusive evidence for or against the Armand correlation. Regarding channel sizes specifically: only a 300 μm microchannel was tested in this study, so definitive size limits for the models were not able to be determined. Furthermore, this study was not an exhaustive test of all void fraction modes, rather, an examination of different categories of models, the influence of their mechanisms, applicability of assumptions, and their most predominantly used correlations.

A limit to testing a wider spread of flow regimes was the relatively low flow rates used in this study. The available syringes and Fisher Scientific syringe pumps limited volumetric flow rates to ~400 mL/hr, so churn and annular flow regimes were not achieved (Fig. 2). Differences in void fraction model accuracies are very likely to occur at these higher intensity, turbulent and mixed flow regimes.

Errors and limitations of video processing prevented all the recorded data from being analyzed. At higher Q_g values, roll wave and 2D wave instabilities were observed in the thin liquid film surrounding the gas core, shown in Figure 14 below [18]. These portions of data were omitted from the analysis because a consistent top/bottom liquid film thickness was not available to reliably measure the void fraction and fulfill the necessary assumptions for data processing.

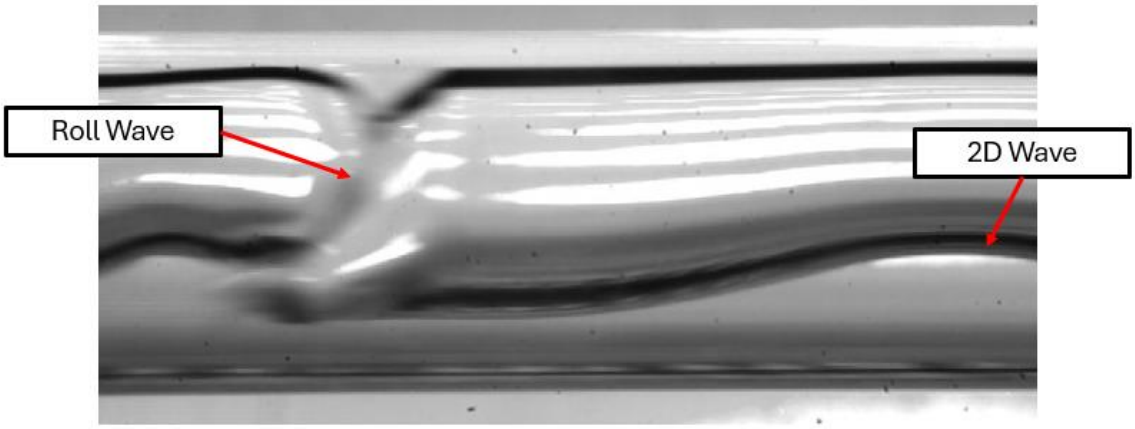

Fig. 14: Film instabilites in experimental data [18].

Lastly, video data analysis could benefit from a higher recording frame rate to most accurately determine the time scales of bubbles passing through the channel. There were segments of data which did not have enough temporal resolution to exactly pinpoint when the bubble entered/exited the test section of the microchannel. Some of these data segments, therefore, may have ±1 frame of error ($\pm 10^{-5}$ seconds at 10,000 frames per second).

4. Conclusions

4.1 Summary of Findings

This study evaluated the predictive abilities of the homogeneous flow model, slip ratio models (Chisholm correlation), drift flux models (Chen et al. correlation), and other empirical equations (Armand correlation) for void fraction in adiabatic two-phase flow. A 300 μm microchannel was used, with air and deionized water at superficial velocites of 0.08-1.5 m/s, resulting in slug and some bubbly flow regimes (Fig 2). It was determined that, for the given experimental conditions, the Armand correlation provided the best predictive model for void fraction α based on homogeneous void fraction β. This model closely matched the strong linear fit of the raw data, had the lowest root-mean-square error of 0.07154, and overall effectively captured the combined influence of flow conditions and mechanisms better than the specialized void fraction models. It is important to note the key limitations of this study are the lack of comprehensive study across all flow regimes, and the lack of definitive channel size limits for which each model may be accurate.

4.2 Future Studies

The most pertinent future study should be determining the upper and lower channel size limits for each model's accuracy. This can be done by simply repeating the experiment with channels of different diameters (most importantly, smaller) and even different cross-sectional geometries (square/rectangular). To this end, more robust pumping equipment should also be used to achieve higher flow rates and observe all flow regimes. Different fluids should be used under varying conditions to examine the effects of viscosity and surface tension on void fraction predictability. Other related work should focus on creating a machine learning model to process image/video data, which will greatly increase the speed and ease of data analysis, essentially removing human time constraints. The end goal of this work is to establish a better understanding of two-phase flow for applications in thermal design, so extensional studies to void fraction in flow boiling (non-adiabatic) systems should be made.

5. Acknowledgements

The author would like to thank the following faculty and associates at the University of Florida, Gainesville, Florida, USA: Dr. Saeed Moghaddam, for his continued support and allowed use of the Nanostructured Energy Systems Laboratories facilites, Drs. Youngsup Song, Matthew J. Traum, and Fernando Mérida, for their involvement with this study, as well as their support in the author's undergraduate studies, and Dr. Adam Kriz and PhD candidate Stephanie Moore, for their mentorship and support.

6. References

[1] Tamvada, S.R., Alipanah, M., and Moghaddam, S., "Membrane-Based Two Phase Heat Sinks for High Heat Flux Electronics and Lasers," *IEEE Transactions on Components, Packaging, and Manufacturing Technology*, Vol. 11, Issue 10, October 2021.

[2] JJ Cooling Innovation, "Two-Phase Flow Heat Transfer: Higher cooling performances," 2024.

[3] Tamvada, S.R. and Moghaddam, S., "Data center energy efficiency enhancement potential of a membrane-assisted phase-change heat sink," *Applied Thermal Engineering*, Vol. 228, June 2023.

[4] Triplett, K.A., Ghiaasiaan, S.M., Abdel-Khalik, S.I., LeMouel, A., and McCord, B.N., "Gas–liquid two-phase flow in microchannels: Part I: void fraction and pressure drop," *International Journal of Multiphase Flow*, Vol. 25, Issue 3, pp. 395-410, April 1999.

[5] Triplett, K.A., Ghiaasiaan, S.M., Abdel-Khalik, S.I., LeMouel, A., and McCord, B.N., "Gas–liquid two-phase flow in microchannels: Part I: void fraction and pressure drop," *International Journal of Multiphase Flow,* Vol. 25, Issue 3, pp. 395-410, April 1999.

[6] Chen, W.L., Twu, M.C., and Pan, C., "Gas–liquid two-phase flow in micro-channels," *International Journal of Multiphase Flow*, Vol. 28, Issue 7, pp. 1235-1247, July 2002.

[7] Kawahara, A., Chung, P.M.-Y., and Kawaji, M., "Investigation of two-phase flow pattern, void fraction and pressure drop in a microchannel," *International Journal of Multiphase Flow*, Vol. 28, Issue 9, pp. 1411-1435, September 2002.

[8] Chung, P.M.-Y., Kawaji, M., Kawahara, A., and Shibata, Y., "Two-Phase Flow Through Square and Circular Microchannels—Effects of Channel Geometry," *Journal of Fluids Engineering,* Vol. 126, Issue 4, pp. 546-552, July 2004.

[9] Chisholm, D. and Rooney, D., "Pressure drop during steam/water flow through orifices," *Journal of Mechanical Engineering Science*, Vol. 16, Issue 5, pp. 353-355, 1974.

[10] He, W., Han, J., Zhao, C., Li, Y., and Bo, H., "Review and Evaluation of Slip-ratio-based Void Fraction Prediction Models," *Institute of Nuclear and New Energy Technology, Tsinghua University*, Beijing, China, 2024.

[11] Woldesemayat, M.A. and Ghajar, A.J., "Comparison of void fraction correlations for different flow patterns in horizontal and upward inclined pipes," *School of Mechanical and Aerospace Engineering, Oklahoma State University*, Stillwater, Oklahoma, USA, 2006.

[12] Suo, M. and Griffith, P., "Two-Phase Flow in Capillary Tubes," *Journal of Fluids Engineering*, Vol. 86, Issue 3, pp. 576-582, September 1964.

[13] Cioncolini, A. and Thome, J.R., "Void fraction prediction in annular two-phase flow," *International Journal of Multiphase Flow*, Vol. 43, pp. 72-84, July 2012.

[14] Armand, A.A. and Treschev, G.G., "The Resistance During the Movement of a Two-Phase System in Horizontal Pipes," *Proceedings of the All-Union Thermal Engineering Institute*, Vol. 1, pp. 16-23, 1946.

[15] Serizawa, A., Feng, Z., and Kawara, Z., "Two-phase flow in microchannels," *Experimental Thermal and Fluid Science,* Vol. 26, Issues 6-7, pp. 703-714, August 2002.

[16] Chung, P.M.-Y. and Kawaji, M., "The effect of channel diameter on adiabatic two-phase flow characteristics in microchannels," *International Journal of Multiphase Flow*, Vol. 30, Issues 7-8, pp. 735-761, July-August 2004.

[17] Chung, P.M.-Y., Kawaji, M., Kawahara, A., and Shibata, Y., "Two-Phase Flow Through Square and Circular Microchannels—Effects of Channel Geometry," *Journal of Fluids Engineering,* Vol. 126, Issue 4, July 2004.

[18] Kriz, A. and Moghaddam, S., "Characterization of inertia- and shear-induced instabilities of liquid films through analysis of wave evolution, energy transfer, and force balance," *Department of Mechanical and Aerospace Engineering, University of Florida,* Gainesville, Florida, USA, 2024.

[19] Traum, M.J., "Beta is a Function of Where You Look," handwritten formulation of analytical homogeneous void fraction model, *Department of Mechanical and Aerospace Engineering, University of Florida*, Gainesville, Florida, USA, 2024.

7. Appendix

7.1 Analytical Derivation: Influence of Axial Location on β

The following side view (Fig. 15) shows the model used for this derivation [19]. The flow enters on the left side, passes through the circular channel of diameter D and length L, then discharges at atmospheric pressure P_{atm}.

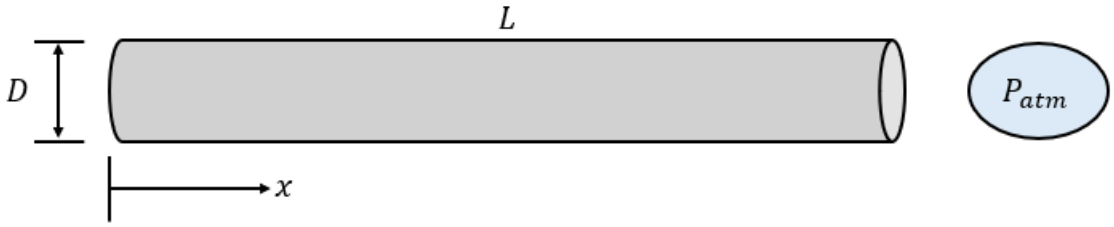

Fig. 15: Diagram for axial location analysis, *adapted from Traum*, 2024 [19]

Applying these conditions to the Darcy-Weisbach pressure drop equation, assuming laminar flow (experimentally verified for all trials), gives the following formulation for the pressure P as a function of x.

$$\Delta P = P(x) - P_{atm} = f\left(\frac{L-x}{D}\right)\frac{\rho\bar{U}^2}{2}$$

$$Re_l = \frac{\rho\bar{U}_l D}{\mu}$$

$$f = \frac{64}{Re} = \frac{64\mu}{\rho\bar{U}_l D}$$

$$P(x) - P_{atm} = \left(\frac{64\mu}{\rho\bar{U}_l D}\right)\left(\frac{L-x}{D}\right)\frac{\rho\bar{U}_l{}^2}{2} = \frac{32\mu}{D^2}\bar{U}_l(L-x)$$

$$Q_l = \bar{U}_l A = \frac{\pi D^2 \bar{U}_l}{4} \rightarrow \bar{U}_l = \frac{4Q_l}{\pi D^2}$$

$$P(x) = \frac{128\mu Q_l}{\pi D^4}(L-x) + P_{atm}$$

For a fixed set of flow rates and temperature, apply the ideal gas law to the gas phase and substitute into the formula for homogeneous void fraction β.

$$Q_g = \frac{\dot{m}_g R_g T}{P(x)} = \frac{constant\ C}{P(x)}$$

$$\beta = \frac{Q_g}{Q_g + Q_l} = \left(1 + \frac{Q_l}{Q_g}\right)^{-1} = \left(1 + \frac{Q_l}{C} P(x)\right)^{-1}$$

$$\beta = \left\{1 + \frac{Q_l}{C}\left[\frac{128\mu Q_l}{\pi D^4}(L - x) + P_{atm}\right]\right\}^{-1}$$

$$Let\ k = \frac{128\mu Q_l}{\pi D^4}$$

$$\beta = \left\{1 + \frac{Q_l}{C} P_{atm} + k(L - x)\right\}^{-1}$$

The highlighted term represents the effect of axial location x on the homogeneous void fraction β due to pressure differences. Evaluating this equation at the channel entrance ($x = 0$) and exit ($x = L$) gives the following results.

$$\beta(x = 0) = \left\{1 + \frac{Q_l}{C} P_{atm} + kL\right\}^{-1}$$

$$\beta(x = L) = \left\{1 + \frac{Q_l}{C} P_{atm}\right\}^{-1}$$

7.2 Implications of Axial Location on β

From the preceding derivation, it can be seen that the effect of axial location, represented by the *k(L-x)* term, on β is only negligible if that term is much smaller than the other terms in the equation. For the tested channel diameter of 300 μm and flow rates 20-380 mL/hr, the axial location term was at least three orders of magnitude smaller than the other terms. Thus, for this experiment, the axial effect could be reasonably ignored. However, calculations revealed that the axial location term becamse significant relative to the other terms in channels smaller than ~275 μm under the tested flow conditions. Thus, repeating this study in smaller channels demands that the axial position of the camera be varied to capture the influence of axial location on the void fraction.